Volume 1 | Number 1 | Jan 2013 | Pages 1–100

Dalton Transactions

An international journal of inorganic chemistry
www.rsc.org/dalton

ROYAL SOCIETY OF CHEMISTRY

This is an *Accepted Manuscript*, which has been through the Royal Society of Chemistry peer review process and has been accepted for publication.

Accepted Manuscripts are published online shortly after acceptance, before technical editing, formatting and proof reading. Using this free service, authors can make their results available to the community, in citable form, before we publish the edited article. We will replace this *Accepted Manuscript* with the edited and formatted *Advance Article* as soon as it is available.

You can find more information about *Accepted Manuscripts* in the **Information for Authors**.

Please note that technical editing may introduce minor changes to the text and/or graphics, which may alter content. The journal's standard **Terms & Conditions** and the **Ethical guidelines** still apply. In no event shall the Royal Society of Chemistry be held responsible for any errors or omissions in this *Accepted Manuscript* or any consequences arising from the use of any information it contains.

ROYAL SOCIETY OF CHEMISTRY

www.rsc.org/dalton

Table of Content

CO_2, H_2O

Calcinations

$RE_3(OH)_6(CO_3)Cl$ RE_3O_4Cl
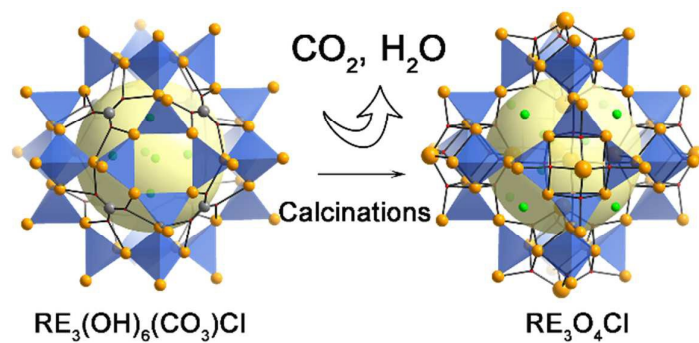
The structural transformation by calcinations and the diluted magnetism of a rare-earth carbonates $RE_3(OH)_6(CO_3)Cl$ with novel SOD topology is reported.

Journal Name

ARTICLE

Sodalite-like Rare-Earth Carbonate: A Study of Structural Transformation and Diluted Magnetism

Yanyan Wang,[a] Tian Han,[a] You-Song Ding,[a] Zhiping Zheng[b] and Yan-Zhen Zheng[a],*

A series of novel rare earth carbonates, $RE_3(OH)_6(CO_3)Cl$ (RE = Dy, Er, Y), with sodalite-like (SOD-like) zeolite topology have been seccessfully synthesized by introducing an appropriate amount of CO_3^{2-} from $NaCO_3$ or atmospheric carbon dioxide as template. Single-crystal X-ray diffraction reveals that the structure consists of the $RE_3(OH)_6^{3+}$ cationic framework with SOD-like topology building from vertex-sharing $[RE_4(\mu_3\text{-}OH)_4]$ cubes. The CO_3^{2-} anions seal on the 6-ring opening and Cl^- anions situate in the channels to achieve charge balance. After calcination at 370 °C, the compound $RE_3(OH)_6(CO_3)Cl$ in-situ transforms into a new phase formulated as RE_3O_4Cl. Interestingly, the strucure of RE_3O_4Cl represents a new SOD-like open framework, associating with the removal of the CO_3^{2-} from $RE_3(OH)_6(CO_3)Cl$. The samples are characterized by thermogravimetric analysis (TGA), elemental analysis, X-ray photoelectron spectroscopy and magnetic study. Furthermore, the single-molecule magnet behaviours can be observed for the diluted samples of $Dy_{0.0068}Y_{2.9932}(OH)_6(CO_3)Cl$ and $Dy_{0.0068}Y_{2.9932}O_4Cl$ with the molar ratio of Dy/Y up to 1/440 as well as $Er_{0.19}Y_{2.81}(OH)_6(CO_3)Cl$ with Er/Y of 1/15, showing the dominant single-ion effects.

Introduction

Open framework materials with porous structure, especially with zeolitic topology, have attracted considerable attentions for their porosity, excellent thermal and chemical stabilities, and are widely used in industrial applications.[1] Among the 229 zeolitic topologies, the traditional zeolite is built exclusively from TO_4 tetrahedra with the T atoms coming from the main group or transition metal group, such as Si^{4+}, Al^{3+}, Ge^{4+}, Zn^{2+}, etc.[2] Rare earth (RE) element is an ideal candidate to incorporate into the open framework materials for the exploration of new applications, since it contains unique properties in photoluminescence, magnetism and so on.[3] Several microporous lanthanide silicates that are built from SiO_4 tetrahedra and LnO_n (n ≥ 6) polyhedra have been successfully prepared.[4]

Moreover, RE ions have become attractive candidates for

constructing new single-ion magnets (SIMs) as well as single-molecular magnets (SMMs), because most of them have a large unquenched orbital angular momentum, which may bring significant anisotropy to the system.[5] Synthetic efforts along this line have led to the discovery of many materials featuring SIM behavior expanding to lanthanide clusters and even complexes with 3-dimentional (3D) metal-organic framework.[6] However, few magnetic studies are focused on RE inorganic materials with 3-dimentional (3D) open framework materials.[7]

The synthesis of traditional open framework materials is typically carried out in a gel medium under solvothermal conditions by using alkali metal ions or organic amines as the templates or structure-directing agents (SDAs).[8] However, this strategy is not accessible to synthesize RE open frameworks as the RE ions have variable and high coordination numbers as well as poor directionality, which is significantly different from the transition metal ions.[9]

For the design of RE open frameworks, it is worthwhile to refer the synthesis of transition or lanthanide-based clusters,[10] in which carbonato (CO_3^{2-}) anion is an extremely versatile bridging ligand. Besides to balance the positive charges of metal ions (3d or 4f), each oxygen atom of CO_3^{2-} anion in the clusters may act as a monodentate, bifunctional, or trifunctional ligand to generate carbonato-bridged complexes.[11] The CO_3^{2-} anion affords various coordination modes, ranging from simple chelation to the more intricate coordination modes (μ_3, μ_4, μ_5 and μ_6), to construct complicated metal-carbonate cores.[12] Therefore, the polycarbonate-lanthanoid cores with diverse structures are highly appropriate to construct special RE compounds with 3-D

a. Centre for Applied Chemical Research, Frontier Institute of Science and Technology, and MOE Key Laboratory for Nonequilibrium Synthesis and Modulation of Condensed Matter, College of Science, Xi'an Jiaotong University, Xi'an 710054, China.
b. Department of Chemistry and Biochemistry, University of Arizona, Tucson, Arizona 85721, USA
Fax: (+) 86-29-83395366
Email: zheng.yanzhen@xjtu.edu.cn

open framework.[13] The CO_3^{2-} anion maybe also act as a SDA in the design of RE compounds with unique structure, since the CO_3^{2-} anion in the carbonates can be easily removed by calcinations.

Herein we present a series of novel rare earth carbonates $RE_3(OH)_6(CO_3)Cl$ (RE = Dy, **1**; Er, **2**; Y, **3**) that exhibit the sodalite-like structure constructed from the building unit (BU) of $[RE_4(\mu_3\text{-}OH)_4]$ cubes by introducing an appropriate amount of CO_3^{2-} from $NaCO_3$ or atmospheric carbon dioxide. Remarkably, the calcinations of **1** at 370 °C leads to the transformation of $Dy_3(OH)_6(CO_3)Cl$ to a new open framework compound, Dy_3O_4Cl (denoted as **1-c**). The structures are solved by single-crystal X-ray diffraction. By diluting **1**, **1-c** and **2** with Y atoms, the interesting dynamic magnetism of three samples (denoted as **1d** $(Dy_{0.0068}Y_{2.9932}(OH)_6(CO_3)Cl)$, **1d-c** $(Dy_{0.0068}Y_{2.9932}O_4Cl)$ and **2d** $(Er_{0.19}Y_{2.81}(OH)_6(CO_3)Cl)$) have been studied.

Results and discussions

Syntheses

Compounds **1**, **2** and **3** were prepared by the hydrothermal reaction of a mixture of $RECl_3\cdot6H_2O$, 2.5 M NaOH, HCl (37 wt%) and H_2O to get a PH value of 6. Finally, Na_2CO_3 was introduced to make a reaction gel of $1.0RECl_3$: $1.2HCl$: $2.5NaOH$: $0.33Na_2CO_3$: $332H_2O$. The gel was added into a 12 mL Teflon-lined stainless steel autoclave and reacted at 200 °C for 72 h. Many parameters including the pH value and reaction temperature were found to affect the formation of $RE_3(OH)_6(CO_3)Cl$. The mixture of HCl and NaOH is used to reach pH = 6 and provide excessive chloride that is benefit for a high yield. Notably, the addition of Na_2CO_3 is essential for the formation of the product. It has been previously shown that the structure of RE clusters and cages are able to be modified by incorporating CO_3^{2-} anions as a template, which is critical for the further aggregation and growth of the product.[14] In this system, the reaction without Na_2CO_3 leads to another RE compound with 2D structure, $RE(OH)_2Cl$, as well as few target crystals. It suggests that the CO_3^{2-} anion is necessary to generate the 3D structure in this reaction, and it may be introduced from atmospheric carbon dioxide. Contrarily, if Na_2CO_3 is added more than the stoichiometric ratio of 0.33, another known RE compound $RE(OH)CO_3$ is obtained, and the yield of this by-product would increase. By further increasing the ratio of Na_2CO_3 to 1, the pure phase of the by-product can be produced. Hence the presence of an appropriate amount of CO_3^{2-} is vital for the syntheses of **1**, **2** and **3**.

Crystal Structure

Single-crystal structure analyses reveal that **1**, **2** and **3** crystallizes in the cubic space group *Im-3*, *Im-3m* and *Im-3m*, respectively (Table S1, S2, S3, ESI†). The asymmetric unit contains 0.5 crystallographically distinct RE sites and 0.16667 crystallographically distinct C sites (Fig. S1, ESI†). Every RE atoms is coordinated with six μ_3-O (O(2) and O(3)) atoms from OH^- in the framework and four O (O(1)) atoms from two μ_6-CO_3^{2-}. Notably, the occupancy of O(1) is half due to the

disorder of CO_3^{2-}. Then the RE atoms are eight-coordinated. The bond distances of Dy-$O_{\mu3}$ in **1** vary from 2.302(11) Å to 2.347(7) Å, of Er-$O_{\mu3}$ in **2** from 2.290(13) Å to 2.328(8) Å and of Y-$O_{\mu3}$ in **3** from 2.333(10) Å to 2.379(6) Å (Table S4, ESI†). The RE-O(1) bond is longer, with average 2.538 Å for Dy-O(1), 2.522 Å for Er-O(1) and 2.565 Å for Y-O(1). The structure and purity of samples are verified by PXRD experiments (Fig. S2).
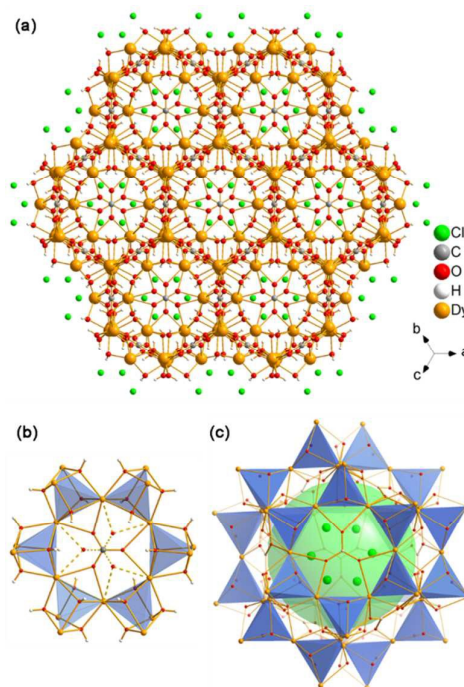
Fig. 1 3-D structure of **1** viewing along the [111] direction.

1, **2** and **3** contain the same structure. Take **1** for example, it consists of the $Dy_3(OH)_6^{3+}$ cationic framework, with CO_3^{2-} anions located in the centre of the 6-ring opening and Cl^- anions in the channels to achieve the charge balance (Fig. 1a). As shown in Fig. 1b, the Dy atoms are linked with each other via six μ_3-OH^-, and each Dy atom belongs to two $[Dy_4(OH)_4]$ units. The $[Dy_4(OH)_4]$ unit is the only BU of the framework. In the centre of the 6-ring opening, a μ_6-CO_3^{2-} ligand binds the six dysprosium ions with a μ_6-η^2:η^2:η^2 bridging mode by way of every O atom of CO_3^{2-} coordinated with two Dy atoms on the 6-ring. The coordination mode of CO_3^{2-} is common in the clusters.[12d] Because of the high symmetry of the structure, the O atoms here are disordered in two places with the occupancy of each one half. The six BUs on the 6-ring opening are linked with each other by vertex-sharing and form a geometry similar to the $\{Ni_{12}\}$ or $\{Mn_{12}\}$ clusters, which is also templated by CO_3^{2-} anions.[15]

Furthermore, an SOD cage can be observed by vertex-sharing of 24 BUs (Fig. 1c). The cage shows six 4-ring openings and eight 6-ring openings, which are composed by four BUs and six BUs, respectively. Each 6-ring opening is sealed by a CO_3^{2-} anion. Cl^- in the cages act as the template here, which is similar to the role of alkali metals or organic amines in the traditional zeolites. Interestingly, the structure of the super

cage is the same as a 60-metal-atom cluster, $[Er_{60}(L\text{-thre})_{34}(\mu_6\text{-}CO_3)_8(\mu_3\text{-OH})_{96}(\mu_2\text{-O})_2(H_2O)_{18}]Br_{12}(ClO_4)_{18}$ $(H_2O)_{40}$ (L-thre = L-threonine), that also possesses sodalite cage featuring 24 vertex-sharing $[Er_4(\mu_3\text{-OH})_4]$ cubes.[16] The core of 60-metal-atom clusters, as well as the {Ni$_{12}$} or {Mn$_{12}$} clusters, are encapsulated in a coordination sphere to be independent. But in this framework, the cages combine with each other to give rise to the 3D structure. In general, the anions, such as CO_3^{2-} and Cl^-, may have a significant function on directing the structure of rare earth. Besides, the triangular coordination geometry of CO_3^{2-} may induce competing magnetic interactions between the metal centres, such as geometrical

spin frustration, which is believed to be beneficial for enhancing magnetocaloric effect.[17]

The $Dy_3(OH)_6^{3+}$ open-framework structure of **1** is built up from DyO$_6$ polyhedron. Such framework is featured by a characteristic body-centred building unit (BU), $[Dy_4O_4]$ cube, as shown in Fig. 2a. Each BU is composed of four Dy and four O atoms connected alternatively. The Dy atoms are located on the vertexes to form a $[Dy_4]$ tetrahedron. The $[Dy_4O_4]$ cube turns to be $[Dy_4]$ tetrahedral node, like the SiO$_4$ or AlO$_4$ tetrahedron as the secondary building unit (SBU) in the zeolite (Fig. 2b). The $[Dy_4]$ tetrahedra linked with each other by vertex (Fig. 2c).
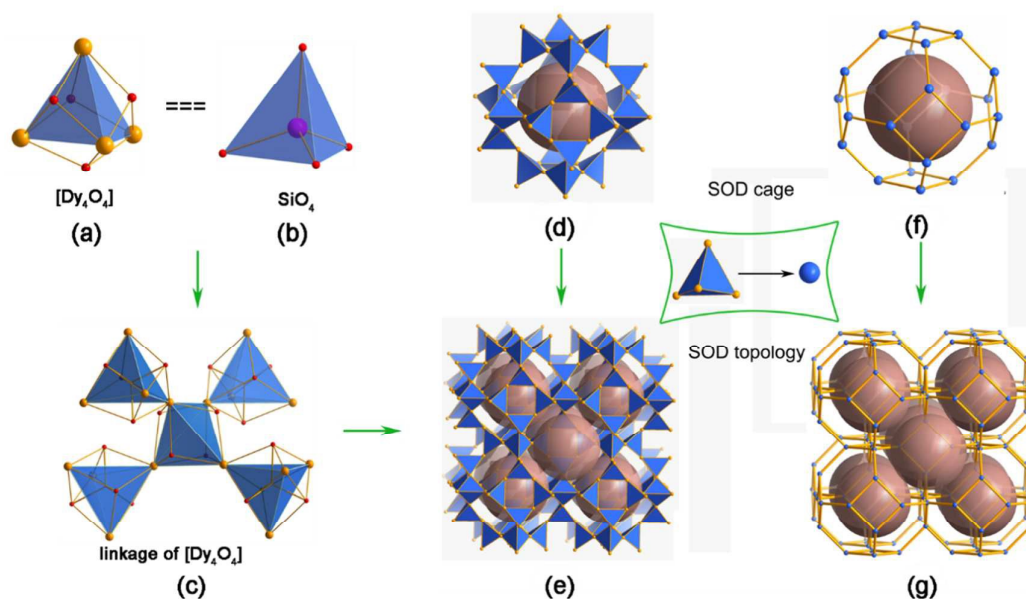
Fig. 2 (a) The Building unit (BU) for the 3-D framework of **1**, $[Dy_4O_4]$; (b) The BU for most zeolites, $[SiO_4]$; (c) The linkage of $[Dy_4O_4]$ BUs in the 3-D framework of **1**; (d) SOD cage linked by 24 $[Dy_4]$ tetrahedral; (e) 3-D framework of **1** connected by sharing 6-ring and 4-ring faces from the SOD cages; (f) The SOD cage derived by taking the $[Dy_4]$ tetrahedron as one tetrahedral node; (g) the SOD topology derived from the structure showing in (e).

To simplify the structure, all of the $O_{\mu3}$ is omitted, as shown in Fig. 2d to Fig. 2g. Firstly, the $[Dy_4]$ tetrahedra linked with each other to give rise to a super cage, which contains 24 $[Dy_4]$ tetrahedra (Fig. 2d). By face-sharing of the SOD-like cages, it constructs into the 3D open framework of **1** (Fig. 2e), which contains 3D intersection channels along the [111], [1$\bar{1}$1], [11$\bar{1}$] and [$\bar{1}$11] directions. If considering the $[Dy_4]$ tetrahedral as a tetrahedral node, the cage is built up by the vertex-sharing of $[Dy_4]$ tetrahedral, which is very similar to the typical sodlite cage (Fig. 2f). The framework of **1** shows a topology of SOD, as shown in Fig. 2g. The free diameters are 4.1 × 4.3 Å^2 (Dy···Dy distance) for the 6-ring channel, which is comparable to those of 8-ring in aluminosilicate zeolites, such as CHA, LEV, LTA, et al. The framework density (FD) of **1** is 12.3 Dy atoms per 1000 Å^3. That is lower than the SOD with FD$_{Si}$ of 16.7 T/1000 Å^3 and comparable to some zeolites with 8-ring channels due to the long distance of Dy-O bond.[18] The SOD topology was firstly found for the mineral sodalite in 1930, and used to be studied in zeolites.[19] Recently, the SOD topology also existed in several ZMOFs or ZIFs.[20] This complex is one of the rare examples

about rare earth with zeolite topology.[21] It may be a guidance to explore new RE compound with zeolite topology by using $[RE_4]$ tetrahedron as building unit.

The framework of **1** can be described as a three-period net with the highest symmetry of *Im*-3*m* containing only one type of T site as determined by the Systre software.[22] The vertex symbol for the T site in the net is $3_6.4.5_4.6_4$. This three-period net is featured by a unique natural tiling with a transitivity of (1 2 3 2). There are two different tiles in this tiling with face symbols of $[3^4]$ and $[3^{24}.4^6.6^8]$. The signature of this tiling is $6[3^4] + [3^{24}.4^6.6^8]$. Considering from the building unit of $[Dy_4(O)_4]$, the framework of **1** also can be described as a three-period net of SOD topology with the highest symmetry of *Im*-3*m*. The vertex symbol for the T site in the net is $4_2.6_4$. This three-period net is carried by a unique natural tiling with a transitivity of (1 1 2 1). There is one type of tile in this tiling with face symbol of $[4^6.6^8]$.

TG analysis has been measured to study the thermal stability of **1**, it shows a total weight loss of 18.6% from 200 to 800 °C with two stages with the first one occurring between

300–450 °C (Fig. S3). Under heating treatment under 370 °C for 4 h, the structure will transform into **1-c**. Surprisingly, the structure of **1-c** can be solved by single-crystal X-ray diffraction. This phenomenon is rarely observed in the RE inorganic compounds. Based on the analysis of single-crystal X-ray diffraction, CO_3^{2-} anions are removed. The space group has transformed into trigonal R-3 for **1-c** from cubic Im-3 for **1**. Besides, some micro variation happens on the structure. Here, we consider the CO_3^{2-} anions are removed by forming CO_2 during the calcinations. From the TG curve, the first stage weight loss of 13.6 wt% occurs around 370 °C, which is corresponding with the removal of CO_2 and H_2O. Then it will give a molecular formula of Dy_3O_4Cl. The possible chemical equation is shown as follows:

$$Dy_3(OH)_6(CO_3)Cl \rightarrow Dy_3O_4Cl + CO_2 + 3H_2O$$

The PXRD pattern of **1-c** corresponds well with the simulated one based on the single-crystal structure of **1-c**, indicating the pure phases of the as-synthesized sample (Fig. S4). The formula of **1-c** is confirmed by ICP, elemental analyses and anion chromatography analysis (Dy, 82.7; C, 0.41; H, 0.92; Cl, 5.95; anal. Calcd. Dy, 83.0; C, 0; H, 0; Cl, 6.04 wt%). Besides, x-ray photoelectron spectroscopy (XPS) of **1** and **1-c** are also measured to verify the existence of Cl. Fig. S5 shows the XPS survey spectra and narrow scan XPS spectra of **1** and **1-c**. The signal around 198 eV is consistent with binding energy of Cl $2p$, indicating the existence of Cl$^-$ in the structures.[23] The content ratio of Dy/Cl for **1** and **1-c** derived from XPS analysis are close to 3, corresponding to the formula of $Dy_3(OH)_6(CO_3)Cl$ and Dy_3O_4Cl, respectively. Besides, the calcinations derivatives (**2-c** and **3-c**) with similar structure can be obtained following the same treatment for **2**, and **3**.

Single-crystal structure analysis of **1-c** reveals that the asymmetric unit contains three crystallographically distinct Dy sites and four crystallographically distinct O sites (Fig. S6, ESI†). Dy(1) and Dy(2) are six-coordinated with six μ_4-O (O(1), O(2), O(3) and O(4)), Dy(3) is seven-coordinated with the four μ_4-O and three Cl atom. The Dy-O$_{\mu 4}$ bond lengths have a reasonable range of 2.13(4) – 2.41(6) Å.

The structure of **1-c** may be subscribed as a cationic framework $Dy_3O_4^+$ with 3D intersection 6-ring channels along the [001], [$\bar{1}$11], [211] and [12$\bar{1}$] directions (Fig. 3a, S7). Cl$^-$ anions are situated in the channels to balance the charge. Comparing with **1**, all of CO_3^{2-} anions have been removed. The 3D open framework of **1-c** is constructed by face-sharing of the super cages, which is similar to **1**, as shown in Fig. 3b. But all of the μ_3-OH in **1** have become μ_4-O in **1-c**. The μ_4-O connect to one Dy(3) atom and three other Dy atoms (Dy(1) and/or Dy(2)) to form anion-centered ODy_4 tetrahedra, which is common in inorganic compounds.[24] By ignoring the Dy(3) atom, the framework of **1-c** also contains vertex-sharing linkage of the [Dy_4] cubes with the same framework of **1**. In the SOD-like cage, [Dy_4] cubes are comprised from all of the Dy(1) and Dy(2) atoms with Dy(3) situated nearby the six 4-ring openings. Then at the two side of the 4-ring opening of the SOD cage, two Dy(3) linked to four [Dy_4O_4] cubes by coordinating with four O

atoms from the four cubes (Fig. 3c). As shown in Fig. 3d, high-resolution TEM images (HRTEM) of **1-c** clearly shows a hexagonal lattice with void distances of 5.9 Å, which corresponds to the distances of the crystallographic planes of (021), ($\bar{2}$01) and (2$\bar{2}$1) (5.883 Å). It further confirms the structure of **1-c**.
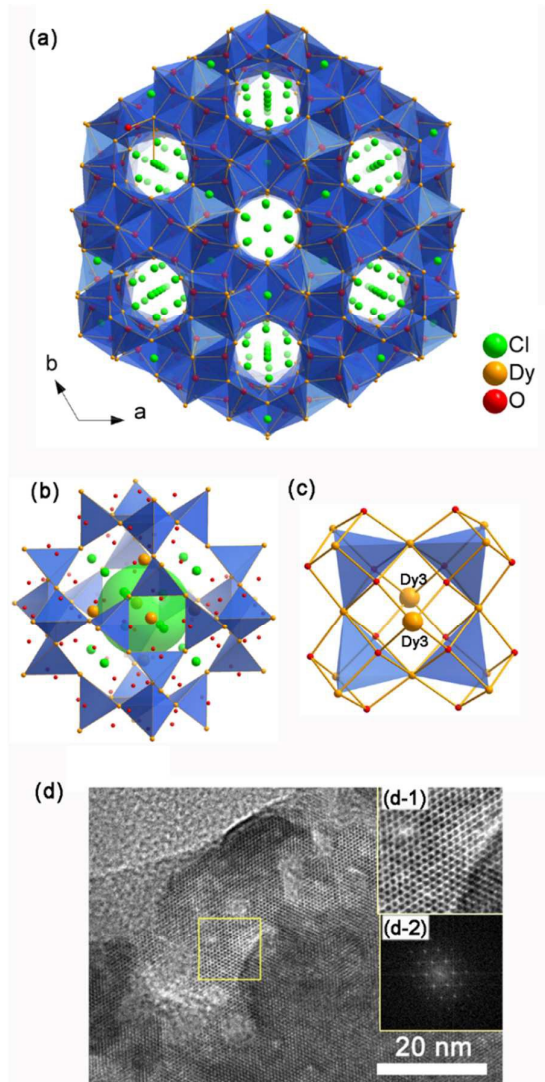
Fig. 3 (a) structure of **1-c** viewed along the [001] direction; (b) super cage linked by 24 [Dy_4] tetrahedra; (c) The coordination between Dy(3) atoms and the 4-ring opening of the super cage; (d) HRTEM micrograph of **6** along the [010] zone axis. Insert: (d-1) enlarged image of the yellow box and corresponding FFT; (d-2) enlarged zones of crystallographic planes of (021), ($\bar{2}$01) and (2$\bar{2}$1) with interplane distances of 5.883 Å.

Magnetic analyses

Dc magnetic susceptibility data of **1**, **1-c** and the corresponding diluted samples (**1d** and **1d-c**, respectively) are measured in the temperature range of 2–300 K (Fig. 4). At 300 K, the $\chi_m T$ products for the samples are 13.90, 13.81, 13.29 and 13.39 cm^3 K mol^{-1} for **1**, **1d**, **1-c** and **1d-c**, respectively, which are compatible with the calculated value of 14.17 cm^3 K mol^{-1} for the ground state of one Dy^{III} ion (4f^9, S = 5/2, L = 5, J =15/2 and

$g = 4/3$) in the free ion approximation. Upon cooling, the $\chi_m T$ products decrease gradually at first and then more rapidly to the minimum at 2 K for all of the compounds.
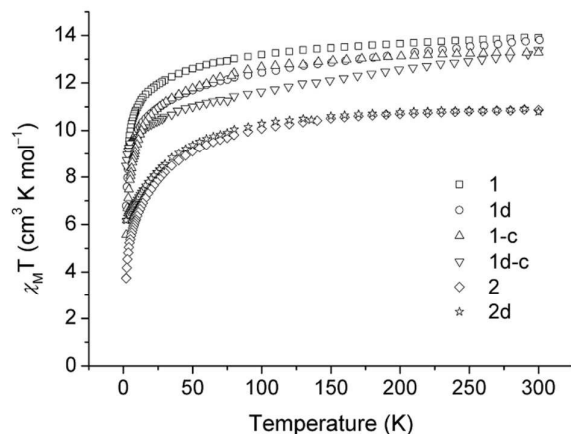
Fig. 4 Experimental $\chi_M T$ product of **1**, **1d**, **1-c**, **1d-c**, **2** and **2d** in an applied field of 2 kOe, 1 kOe, 1 kOe, 1 kOe, 0.5 KOe and 1 KOe for **1**, **1d**, **1-c** , **1d-c**, **2** and **2d**, respectively. The $\chi_M T$ curve has been rescaled for one RE^{III} ion.

The $\chi_m T$ *versus* T plots for compounds **2** and **2d** are recorded between 2 and 300 K under a dc field of 500 Oe and 1 kOe, respectively (Fig. 4). The $\chi_m T$ values at room temperature are 10.87 and 10.80 for **2** and **2d**, respectively, which are close to the expected value of 11.48 cm^3 K mol^{-1} for one Er^{III} ion (4f^{12}, S = 3/2, L = 6, J =15/2 and g = 6/5). In the high-temperature range, the $\chi_m T$ product decreases slowly upon cooling for both compounds; below 75 K, the $\chi_m T$ product drops quickly to the minimum of 3.74 cm^3 K mol^{-1} at 2 K for **2**, and a minimum value of 6.17 cm^3 K mol^{-1} for the diluted sample of **2d**.

The magnetization *versus* field plots are determined at low temperatures in the range of 0–70 kOe, as shown in Fig. S8. For **1** and **1c**, the magnetizations at 2 K increase continuously upon an increase of the magnetic field, reaching the maxima of 5.57 $N\beta$ and 5.04 $N\beta$ for **1** and **1-c**, respectively. These obtained values are far from the saturated magnetization for one Dy^{III} ion but in agreement with the data reported previously as a result of the large magneto-anisotropy and/or the low lying excited states of the Dy^{III} ion. For **2**, similar behavior of the field-dependent magnetization is observed, with the highest product of 4.46 $N\beta$ at 2 K, which is again without saturation and possibly because of the presence of large magnetic anisotropy.

The alternative current (ac) susceptibility were performed on the microcrystalline samples to investigate the dynamic behaviour of the magnetization at low temperatures, as displayed in Fig. S9. For **1**, **1-c** and **2**, curves based on in-phase and out-of-phase signals of ac susceptibility are all superimposed on a nearly single–master curve, whether in the absence of an external dc field or even at an applied dc field of 1 kOe. This phenomenon often exists in the high-nuclearity lanthanide cages, that probably due to the crowded distribution of metal ions in high-nuclearity clusters, as well as in the titled complexes.[25]
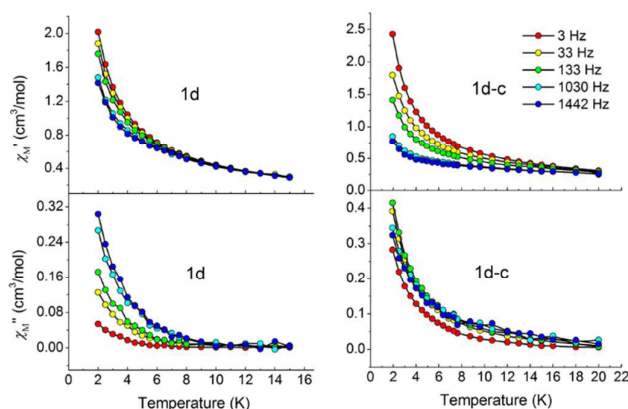
Fig. 5 In-phase (up) and out-of-phase (down) dynamic susceptibility of **1d** and **1d-c** without external dc magnetic fields. Solid lines are included to guide the eyes.

Magnetic dilution may promote the slow magnetic relaxation U_{eff} originating from SIM behaviour in mononuclear and polymeric compounds, such as 1D dysprosium chain, 2D layer, and even 3D LiYF$_4$.[26] It is just the advantage here to study the magnetism of the samples with very large dilution ratios up to 0.227 %, under which the magnetic signal is still precluded by the instrument sensitivity for **1** and **1-c**, while that cannot be detected for most of the diluted sample reported. Therefore, the doped samples **1d** and **1d-c** in Dy:Y molar ratios of 1:440 are prepared to examine the nature of magnetism. As shown in Fig. 5, ac measurements for both diluted samples in zero dc field show obvious frequency dependence below 8 K, an indication of slow relaxation of the magnetization. But unfortunately, no maximum is observed in both in-phase and out-of-phase signals of ac susceptibility, possibly due to the presence of a fast relaxation of the magnetisation through a quantum tunnelling mechanism. Thus, ac measurements are taken in an application of a small external dc field of 500 Oe to mitigate the quantum tunnelling (Fig. S10). Significant frequency-dependent χ' and χ'' signals appears for both compounds and a maximum in χ' is clearly observed moving to higher temperature towards higher frequency especially for **1d**, indicating an SIM behaviour.

For **2**, similar phenomenon has occurred (Fig. S11). The doped sample **2d** with Dy:Y molar ratio of 1:15 shows slow relaxation of the magnetization under 1 kOe dc field, proving the position effect of dilution of open framework materials on the SIM behaviour once again. All the information points out that such slow relaxation is likely dominated by the single ion effects, and vanishes when more of the lanthanide ions are incorporated. The magnetic exchange interaction, although it is weak between lanthanides, and dipolar interaction, as well as the orientation of the easy axes of magnetization work together in the molecular architecture, leading to a complicated situation which is not beneficial to the SIM behaviour.

Conclusions

In conclusion, we have successfully synthesized a series of novel rare earth carbonates $RE_3(OH)_6(CO_3)Cl$ (RE = Dy (**1**), Er (**2**), Y (**3**)) with SOD-like structure building from $[RE_4(\mu_3\text{-}OH)_4]$ cubes by introducing CO_3^{2-} for the first time. Interestingly, the CO_3^{2-} can be the removed after calcination at 370 °C. And the single-crystal of **1** can be in-situ transformed into a new zeolitic compound Dy_3O_4Cl (**1-c**) with two Dy atoms located at both sides of the 4-ring on the SOD-like structure. Magnetic studies of both diluted samples of **1** and **1-c** exhibit SIM-type behaviours. As such, both diluted compounds can be safely labelled as $M^0U^0S^3$ according to their magneto-structural correlations.[27] These results provide a guidance on the syntheses of RE-based open frameworks, and promisingly open a new door towards diluted magnets.

Experimental section

Reagents and solvents were commercially available and used as received without further purification.

Synthetic procedures

Synthesis of $Dy_3(OH)_6(CO_3)Cl$ (1). Typically, dysprosium (III) chloride hexahydrate ($DyCl_3 \cdot 6H_2O$, 1 mmol) was dispersed into 5 mL distilled water, and fully dissolved by adding 0.1 mL hydrochloric acid (37 wt%, 1.2 mmol). Then 1 mL NaOH solution (2.5 mol L^{-1}) was added to the mixture with stirring for 1 h to get a pH value of 6. Finally, Na_2CO_3 was introduced to make a reaction gel of $1.0DyCl_3$: $1.2HCl$: $2.5NaOH$: $0.33Na_2CO_3$: $332H_2O$. About 1 h later, the gel was added into a 12 mL Teflon-lined stainless steel autoclave and heated at 200 °C for 72 h, followed by cooling to room temperature for 20 h. The white pure crystals were obtained by washing in distilled water for several times and dried at room temperature overnight after filtration. Yield: 176 mg (77 % based on Dy). Elemental analysis of the product gave (in wt.%) Dy: 70.9 (calcd. Dy: 71.2), C: 1.84 (calcd. C: 1.75), H: 1.21 (calcd. H: 0.876), and anion chromatography analysis gave (in wt.%) Cl: 5.11 (calcd. Cl: 5.18), which were consistent with the elemental contents calculated from the molecular formula of $Dy_3(OH)_6(CO_3)Cl$.

Synthesis of $Er_3(OH)_6(CO_3)Cl$ (2). Compound **2** was synthesized following a method similar to that of **1**, using erbium (III) chloride hexahydrate ($ErCl_3 \cdot 6H_2O$) instead of $DyCl_3 \cdot 6H_2O$ to make a reaction gel of $1.0ErCl_3$: $1.2HCl$: $2.5NaOH$: $0.33Na_2CO_3$: $332H_2O$. The product was obtained with a yield of 53 % based on Er with the molecular formula of $Er_3(OH)_6(CO_3)Cl$.

Synthesis of $Y_3(OH)_6(CO_3)Cl$ (3). Compound **3** was synthesized following a method similar to that of **1**, using yttrium (III) chloride hexahydrate ($YCl_3 \cdot 6H_2O$) instead of $DyCl_3 \cdot 6H_2O$ to make a reaction gel of $1.0YCl_3$: $1.2HCl$: $2.5NaOH$: $0.33Na_2CO_3$: $332H_2O$. The product was obtained with a yield of 80 % based on Y with the molecular formula of $Y_3(OH)_6(CO_3)Cl$.

Synthesis of $Dy_{0.0068}Y_{2.9932}(OH)_6(CO_3)Cl$ (1d, 0.227% diluted sample of 1). $DyCl_3 \cdot 6H_2O/YCl_3 \cdot 6H_2O$ (in a 1:449 molar ration; 10 mmol in total) was dispersed into 50mL water, along with 1

mL hydrochloric acid (37 wt%, 12 mmol) added. Then 10 mL NaOH (2.5 mol L^{-1}) was added to the mixture with stirring for 1 h to get a pH value of 6. Finally, Na_2CO_3 was introduced to make a reaction gel of $0.002DyCl_3$: $0.998YCl_3$: $1.2HCl$: $2.5NaOH$: $0.33Na_2CO_3$: $332H_2O$. About 1 h later, the gel was added into a 100 mL Teflon-lined stainless steel autoclave and heated at 200 °C for 72 h, followed by cooling to room temperature for 20 h. pure crystals of **1d** were obtained after washing the product in distilled water and dried at room temperature overnight. The Dy/Y ratio of the product based on ICP analysis (in wt.%) Dy: 0.238, Y: 57.2, gave the molecular formula of $Dy_{0.0068}Y_{2.9932}(OH)_6(CO_3)Cl$.

Synthesis of $Er_{0.19}Y_{2.81}(OH)_6(CO_3)Cl$ (2d, 6.25% diluted sample of 2). Compound **2d** was synthesized following a method similar to that of **1d**, using erbium (III) chloride hexahydrate ($ErCl_3 \cdot 6H_2O$) instead of $0.06ErCl_3$: $0.94YCl_3$:$1.2HCl$: $2.5NaOH$: $0.33Na_2CO_3$: $332H_2O$. The Er/Y ratio of the product based on ICP analysis (in wt.%) Er: 6.63, Y: 52.1, gave the molecular formula of $Er_{0.19}Y_{2.81}(OH)_6(CO_3)Cl$.

Preparation of Dy_3O_4Cl (1-c, the calcined sample from 1). The as-synthesized **1** was placed into a normal furnace and heated from RT to 370 °C at a temperature ramp rate of 1 °C min^{-1} in air with a 4 h isothermal hold at 370 °C before cooling to room temperature at a rate of 1 °C min^{-1}. The transformation of the structure was occurring in this process. The composition of **1-c** is studied by ICP, elemental analyses and anion chromatography analyses (Dy, 82.7; C, 0.41; H, 0.92; Cl, 5.95; anal. Calcd. Dy, 83.0; C, 0; H, 0; Cl, 6.04 wt%). Single-crystal analysis show **1-c** exhibits a new structure. Besides, the calcinations derivatives (**2-c** and **3-c**) with a similar structure can also be obtained following the same treatment of **2**, and **3**. The structure and purity of samples are confirmed by PXRD.

Preparation of $Dy_{0.0068}Y_{2.9932}O_4Cl$ (1d-c, 0.227% diluted sample of 1-c). The as-synthesized **1d** was placed into a normal furnace and treated following the method similar to **1-c**. The structure of **1d-c** are confirmed by PXRD.

Characterization Methods

PXRD data were collected on a Rigaku SmartLab(3) diffractometer with Cu Kα radiation (λ = 1.5418 Å). Inductively coupled plasma (ICP) analysis was performed on a Perkin-Elmer Optima 3300DV spectrometer. Elemental analysis was conducted on a Vario MICRO elemental analyzer. Anion chromatography analysis was performed on DX-500 Ion Chromatography (IC) System of Dionex. Thermogravimetric analysis (TGA) was carried out on a TA Q500 analyzer in air with a heating rate of 10°C min^{-1} from RT to 800°C. X-ray photoelectron spectroscopy (XPS) measurements were performed using a Thermo Escalab 250 spectrometer with monochromatized Al Kα excitation. The TEM and HRTEM images were taken on a JEOL JEM-3010 transmission electron microscope operating at an accelerating voltage of 300 kV. Magnetic measurements were performed on a Quantum Design MPMS XL-7 SQUID magnetometer on polycrystalline samples. Diamagnetic corrections were made with Pascal's constants for all the constituent atoms and sample holder.

Alternating-current (ac) magnetic susceptibility data were collected on the same instrument employing a 3.5 Oe oscillating field at frequencies up to 1442 Hz.

X-ray crystallographic analyses

Suitable single crystal of $Dy_3(OH)_6(CO_3)Cl$ (**1**), $Er_3(OH)_6(CO_3)Cl$ (**2**), $Y_3(OH)_6(CO_3)Cl$ (**3**) and $Dy_3O_5Cl_{0.5}H_{1.5}$ (**1-c**) with dimensions of $0.32 \times 0.21 \times 0.15$, $0.07 \times 0.07 \times 0.05$, $0.05 \times 0.05 \times 0.05$ and $0.06 \times 0.06 \times 0.03$ mm^3, respectively, were selected for single-crystal X-ray diffraction analyses. The intensity data were collected on a Bruker Apex Ⅱ DUO area-detector diffractometer with graphite-monochromated Mo Kα radiation (λ = 0.71073 Å) at temperature of 23 ± 2 °C. Cell refinement and data reduction were accomplished with the SAINT processing program.[28] The structures were solved by direct methods and refined by full matrix least-squares technique with the SHELXTL crystallographic software package.[29] The heaviest atoms of Dy, Er, Y, O, Cl and C could be unambiguously located. The H atoms in the structures of **1**, **2** and **3** were added theoretically, and that of **1-c** were not added. All non-hydrogen atoms were refined anisotropically. CCDC 1416221–1416224 contain the supplementary crystallographic data for this paper. Crystal data and refinement parameters for the structure determination are presented in Table S1–3 and Table S5. The selected bond distances are listed in the Table S4.

Acknowledgements

Notes and references

1 (a) A. Corma, *Chem. Rev.*, 1997, **97**, 2373–2420; (b) J. Li, A. Corma and J. Yu, *Chem. Soc. Rev.*, 2015, DOI: 10.1039/C5CS00023H; (c) Y. Li and J. Yu, *Chem. Rev.*, 2014, **114**, 7268–7316.

2 C. Baerlocher and L. B. McCusker, Database of Zeolite Structures: http://www.iza-structure.org/databases/.

3 (a) G. Yang, Y. Wang, D. Zhou, J. Zhuang, X. Liu, X. Han and X. Bao, *J. Chem. Phys.*, 2003, **119**, 9765–9770; (b) N. Rahimi and R. Karimzadeh, *Appl. Catal., A*, 2011, **398**, 1–17; (c) M. Iwasaki and H. Shinjoh, *Chem. Commun.*, 2011, **47**, 3966–3968; (d) S. Kim, E. Sasmaz and J. Lauterbach, *Appl. Catal., B*, 2015, **168–169**, 212–219.

4 (a) D. Ananias, F. A. Almeida Paz, L. D. Carlos, C. F. G. C. Geraldes and J. Rocha, *Angew. Chem. Int. Ed.*, 2006, **45**,

7938–7942; (b) X. Wang, J. Li, Y. Han, Y. Li, J. Yu and R. Xu, *Chem. Mat.*, 2011, **23**, 2842–2847.

5 (a) N. Ishikawa, M. Sugita, T. Ishikawa, S. Koshihara and Y. Kaizu, *J. Am. Chem. Soc.*, 2003, **125**, 8694–8695; (b) L. Sorace, C. Benelli and D. Gatteschi, *Chem. Soc. Rev.*, 2011, **40**, 3092–3104; (c) Y.-L. Wang, Y. Ma, X. Yang, J. Tang, P. Cheng, Q.-L. Wang, L.-C. Li and D.-Z. Liao, *Inorg. Chem.*, 2013, **52**, 7380–7386.

6 (a) M. Mannini, F. Pineider, C. Danieli, F. Totti, L. Sorace, P. Sainctavit, M. A. Arrio, E. Otero, L. Joly, J. C. Cezar, A. Cornia and R. Sessoli, *Nature*, 2010, **468**, 417–421; (b) S. Cardona-Serra, J. M. Clemente-Juan, E. Coronado, A. Gaita-Ariño, A. Camón, M. Evangelisti, F. Luis, M. J. Martínez-Pérez and J. Sesé, *J. Am. Chem. Soc.*, 2012, **134**, 14982–14990; (c) D. N. Woodruff, R. E. P. Winpenny and R. A. Layfield, *Chem. Rev.*, 2013, **113**, 5110–5148; (d) H. Miyasaka, K. Nakata, K.-i. Sugiura, M. Yamashita and R. Clérac, *Angew. Chem. Int. Ed.*, 2004, **43**, 707–711; (e) I.-R. Jeon and R. Clerac, *Dalton T.*, 2012, **41**, 9569–9586; (f) J. J. Baldoví, E. Coronado, A. Gaita-Ariño, C. Gamer, M. Giménez-Marqués and G. Mínguez Espallargas, *Chem. Eur. J.*, 2014, **20**, 10695–10702.

7 (a) R. Giraud, W. Wernsdorfer, A. M. Tkachuk, D. Mailly and B. Barbara, *Physical Review Letters*, 2001, **87**, 057203; (b) M. Wu, F. Jiang, X. Kong, D. Yuan, L. Long, S. A. Al-Thabaiti and M. Hong, *Chem. Sci.*, 2013, **4**, 3104–3109; (c) M. Wu, F. Jiang, D. Yuan, J. Pang, J. Qian, S. A. Al-Thabaiti and M. Hong, *Chem. Commun.*, 2014, **50**, 1113–1115.

8 J. Yu and R. Xu, *Acc. Chem. Res.*, 2010, **43**, 1195–1204.

9 M. Wu, F. Jiang, X. Kong, D. Yuan, L. Long, S. A. Al-Thabaiti and M. Hong, *Chem. Sci.*, 2013, **4**, 3104–3109.

10 (a) X.-B. Han, Y.-G. Li, Z.-M. Zhang, H.-Q. Tan, Y. Lu and E.-B. Wang, *J. Am. Chem. Soc.*, 2015, **137**, 5486–5493 (b) J. C. G. Bunzli, *Coordin. Chem. Rev.*, 2015, **293**, 19–47; (c) V. Velasco, D. Aguila, L. A. Barrios, I. Borilovic, O. Roubeau, J. Ribas-Arino, M. Fumanal, S. J. Teat and G. Aromi, *Chem. Sci.*, 2015, **6**, 123–131; (d) Y. Zhang, L. Huang, H. Miao, H. X. Wan, H. Mei, Y. Liu and Y. Xu, *Chem-Eur. J.*, 2015, **21**, 3234–3241.

11 A. S. R. Chesman, D. R. Turner, B. Moubaraki, K. S. Murray, G. B. Deacon and S. R. Batten, *Chem-Eur. J.*, 2009, **15**, 5203–5207.

12 (a) A. S. R. Chesman, D. R. Turner, B. Moubaraki, K. S. Murray, G. B. Deacon and S. R. Batten, *Chem-Eur. J.*, 2009, **15**, 5203–5207; (b) B. Zhang, X. Zheng, H. Su, Y. Zhu, C. Du and M. Song, *Dalton T.*, 2013, **42**, 8571–8574; (c) K.-C. Xiong, F.-L. Jiang, Y.-L. Gai, D.-Q. Yuan, D. Han, J. Ma, S.-Q. Zhang and M.-C. Hong, *Chem-Eur. J.*, 2012, **18**, 5536–5540; (d) R. McLellan, J. Reze, S. M. Taylor, R. D. McIntosh, E. K. Brechin and S. J. Dalgarno, *Chem. Commun.*, 2014, **50**, 2202–2204.

13 (a) S. K. Langley, B. Moubaraki and K. S. Murray, *Inorg. Chem.*, 2012, **51**, 3947–3949; (b) R. Sen, D. K. Hazra, M. Mukherjee and S. Koner, *Eur. J. Inorg. Chem.*, 2011, **2011**, 2826–2831.

14 P. C. Andrews, T. Beck, C. M. Forsyth, B. H. Fraser, P. C. Junk, M. Massi and P. W. Roesky, *Dalton T.*, 2007, 5651–5654.

15 G. J. T. Cooper, G. N. Newton, P. Kögerler, D.-L. Long, L. Engelhardt, M. Luban and L. Cronin, *Angew. Chem. Int. Ed.*, 2007, **46**, 1340–1344.

16 X.-J. Kong, Y. Wu, L.-S. Long, L.-S. Zheng and Z. Zheng, *J. Am. Chem. Soc.*, 2009, **131**, 6918–6919.

17 (a) Y. Zheng, A. Ellern and P. Kogerler, *Acta Cryst.*, 2011, **67**, i56–i58; (b) Z. Fu, Y. Zheng, Y. Xiao, S. Bedanta, A. Senyshyn, G. G. Simeoni, Y. Su, U. Rücker, P. Kögerler and T. Brückel, *Phys. Rev. B*, 2013, **87**, 214406; (c) Y.-C. Chen, L. Qin, Z.-S. Meng, D.-F. Yang, C. Wu, Z. Fu, Y.-Z. Zheng, J.-L. Liu, R. Tarasenko, M. Orendac, J. Prokleska, V. Sechovsky and M.-L. Tong, *J. Mater. Chem. A*, 2014, **2**, 9851–9858; (d) Y.-Z. Zheng, G.-J. Zhou, Z. Zheng and R. E. P. Winpenny, *Chem. Soc. Rev.*, 2014, **43**, 1462–1475.

18 (a) X. Song, Y. Li, L. Gan, Z. Wang, J. Yu and R. Xu, *Angew. Chem. Int. Ed.*, 2009, **48**, 314–317; (b) Y. Wang, Y. Li, Y. Yan, J. Xu, B. Guan, Q. Wang, J. Li and J. Yu, *Chem. Commun.*, 2013, **49**, 9006–9008.

19 L. Pauling, *Z. Kristallogr.*, 1930, **74**, 213–225.

20 (a) L. Sun, H. Xing, Z. Liang, J. Yu and R. Xu, *Chem. Commun.*, 2013, **49**, 11155–11157; (b) Y. Ban , Y. Li, Y. Peng , H. Jin , W. Jiao , X. Liu and W. Yang, *Chem-Eur. J.*, 2014, **20**, 11402–11409; (c) C. -T. He, L. Jiang, Z. –Mi. Ye, R. Krishna, Z. -S. Zhong, P. -Q. Liao, J. Xu, G. Ouyang, J. -P. Zhang, and X. -M. Chen *J. Am. Chem. Soc.*, 2015, **137**, 7217–7223.

21 L. F. Wang, H. Li, G. S. Zhu, H. Ren, F. X. Sun and S. L. Qiu, *Chem. J. Chin. Univ.-Chin.*, 2008, **29**, 2127–2130.

22 O. Delgado-Friedrichs, M. O'Keeffe, *Acta Crystallogr., Sect. A* 2003, **59**, 351.

23 (a) The Handbook of X-ray Photoelectron Spectroscopy, Perkin Elmer Corporation, 1979; (b) H. Xing, W. Yang, T. Su, Y. Li, J. Xu, T. Nakano, J. Yu and R. Xu, *Angew. Chem. Int. Ed.*, 2010, **49**, 2328−2331.

24 S. V. Krivovichev, O. Mentré, O. I. Siidra, M. Colmont and S. K. Filatov, *Chem. Rev.*, 2013, **113**, 6459–6535.

25 M. Wu, F. Jiang, X. Kong, D. Yuan, L. Long, S. A. Al-Thabaiti and M. Hong, *Chem. Sci.*, 2013, **4**, 3104–3109.

26 (a) Q. Chen, Y.-S. Meng, Y.-Q. Zhang, S.-D. Jiang, H.-L. Sun and S. Gao, *Chem. Commun.*, 2014, **50**, 10434–10437; (b) D.-D. Yin, Q. Chen, Y.-S. Meng, H.-L. Sun, Y.-Q. Zhang and S. Gao, *Chem. Sci.*, 2015, **6**, 3095–3101; (c) B. Monteiro, J. T. Coutinho, C. C. L. Pereira, L. C. J. Pereira, J. Marçalo, M. Almeida, J. J. Baldoví, E. Coronado and A. Gaita-Ariño, *Inorg. Chem.*, 2015, **54**, 1949–1957; (d) T. Han, J.-D. Leng, Y.-S. Ding, Y. Wang, Z. Zheng and Y.-Z. Zheng, *Dalton T.*, 2015, **44**, 13480–13484; (e) J. A. Quilliam, S. Meng and J. B. Kycia, *Phys. Rev. B*, 2012, **85**, 184415.

27 Y.-Z. Zheng, Z. Zheng, X.-M. Chen, *Coord. Chem. Rev.*, 2014, **258**–**259**, 1–15.

28 SAINT, Bruker AXS Inc., 5465 East Cheryl Parkway, Madison, WI, 53711–5373, USA, 2000.

29 SHELXTL, Bruker AXS Inc., 5465 East Cheryl Parkway, Madison, WI, 53711–5373, USA, 2000.

Supporting Information for

Sodalite-like Rare-Earth Carbonate: A Study of Structural Transformation and Diluted Magnetism

Yanyan Wang,[a] Tian Han,[a] You-Song Ding,[a] Zhiping Zheng[b] and Yan-Zhen Zheng[a],*

[a] Centre for Applied Chemical Research, Frontier Institute of Science and Technology, and MOE Key Laboratory for Nonequilibrium Synthesis and Modulation of Condensed Matter, College of Science, Xi'an Jiaotong University, Xi'an 710054, China.

[b] Department of Chemistry and Biochemistry, University of Arizona, Tucson, Arizona 85721, USA

*To whom correspondence should be addressed. *Email: zheng.yanzhen@xjtu.edu.cn

Table of Contents

Table S1. Crystal data and structure refinement for 1a.

Compound	1
Empirical formula	$CH_6ClDy_3O_9$
Formula weight	685.01
Temperature	296(2) K
Wavelength (Å)	0.71073
Crystal system, space group	Cubic, *Im*-3
Unit cell dimensions	
a (Å)	12.4754(6)
b (Å)	12.4754(6)
c (Å)	12.4754(6)
α (°)	90
β (°)	90
γ (°)	90
Volume (Å^3)	1941.62(16)
Z, calculated density (mg m^{-3})	8, 4.687
Absorption coefficient (mm^{-1})	23.150
F(000)	2392
Crystal size (mm^3)	$0.32 \times 0.21 \times 0.15$
θ range (°) for data collection	$2.31 - 27.46$
Limiting indices	$-13 \leq h \leq 16, -16 \leq k \leq 15, -16 \leq l \leq 12$
Reflections collected/unique	8032/426, [R_{int} = 0.0272]
Completeness to θ (%)	27.46, 100.0
Absorption correction	Semi-empirical from equivalents
Max and min transmission	0.1288 and 0.0505
Refinement method	Full-matrix least-squares on F^2
Data/restraints/parameters	426/7/32
Goodness-of-fit on F^2	0.989
Final *R* indices [$I > 2\sigma(I)$]	$R_1 = 0.0395, wR_2 = 0.1005$
R indices (all data)	$R_1 = 0.0401, wR_2 = 0.1010$
Largest diff. peak and hole (e Å^{-3})	3.028 and −2.256

[a] $R_1 = \sum(\Delta F/\sum(F_o))$, $wR_2 = (\sum[w(F_o^2 - F_c^2)])/\sum[w(F_o^2)^2]^{1/2}$ and $w = 1/\sigma^2(F_o^2)$.

3

Table S2. Crystal data and structure refinement for **2**[a].

Compound	2
Empirical formula	$CH_6ClEr_3O_9$
Formula weight	699.29
Temperature	296(2) K
Wavelength (Å)	0.71073
Crystal system, space group	Cubic, *Im*-3*m*
Unit cell dimensions	
a (Å)	12.4127(4)
b (Å)	12.4127(4)
c (Å)	12.4127(4)
α (°)	90
β (°)	90
γ (°)	90
Volume ($Å^3$)	1912.49(11)
Z, calculated density (mg m^{-3})	8, 4.857
Absorption coefficient (mm^{-1})	26.389
F(000)	2440
Crystal size (mm^3)	$0.07 \times 0.07 \times 0.05$
θ range (°) for data collection	2.32 − 27.49
Limiting indices	$-10 \leq h \leq 9, -4 \leq k \leq 16, -12 \leq l \leq 16$
Reflections collected/unique	1614/252, [R_{int} = 0.0199]
Completeness to θ (%)	27.49, 100.0
Absorption correction	Semi-empirical from equivalents
Max and min transmission	0.3521 and 0.2595
Refinement method	Full-matrix least-squares on F^2
Data/restraints/parameters	252/7/21
Goodness-of-fit on F^2	1.115
Final *R* indices [$I > 2\sigma(I)$]	R_1 = 0.0490, wR_2 = 0.1261
R indices (all data)	R_1 = 0.0553, wR_2 = 0.1313
Largest diff. peak and hole (e Å^{-3})	3.584 and −3.019

[a] $R_1 = \sum(\Delta F/\sum(F_o))$, $wR_2 = (\sum[w(F_o{}^2 - F_c{}^2)])/\sum[w(F_o{}^2)^2]^{1/2}$ and $w = 1/\sigma^2(F_o{}^2)$.

4

Table S3. Crystal data and structure refinement for **3**[a].

Compound	**3**
Empirical formula	$CH_6ClY_3O_9$
Formula weight	464.24
Temperature	296(2) K
Wavelength (Å)	0.71073
Crystal system, space group	Cubic, *Im*-3*m*
Unit cell dimensions	
a (Å)	12.665(9)
b (Å)	12.665(9)
c (Å)	12.665(9)
α (°)	90
β (°)	90
γ (°)	90
Volume (Å^3)	2032(2)
Z, calculated density (mg m^{-3})	8, 3.035
Absorption coefficient (mm^{-1})	17.281
F(000)	1744
Crystal size (mm^3)	0.05 × 0.05 × 0.05
θ range (°) for data collection	2.27 – 26.90
Limiting indices	$-16 \leq h \leq 5, -14 \leq k \leq 15, -11 \leq l \leq 7$
Reflections collected/unique	2253/251, [R_{int} = 0.0526]
Completeness to *θ* (%)	26.90, 99.6
Absorption correction	Semi-empirical from equivalents
Max and min transmission	0.4787 and 0.4787
Refinement method	Full-matrix least-squares on F^2
Data/restraints/parameters	251/7/21
Goodness-of-fit on F^2	1.117
Final *R* indices [$I > 2\sigma(I)$]	R_1 = 0.0701, wR_2 = 0.1868
R indices (all data)	R_1 = 0.0884, wR_2 = 0.2061
Largest diff. peak and hole (e Å^{-3})	2.923 and -1.350

[a] $R_1 = \sum(\Delta F/\sum(F_o))$, $wR_2 = (\sum[w(F_o^2 - F_c^2)])/\sum[w(F_o^2)^2]^{1/2}$ and $w = 1/\sigma^2(F_o^2)$.

Table S4. Selected bond lengths [Å] for **1**, **2**, **3** and **1-c**.

1		2		3		1-c	
Dy(1)-O(2)	2.304(11)	Er(1)-O(2)	2.290(13)	Y(1)-O(2)	2.333(10)	Dy(1)-O(1)	2.34(5)
Dy(1)-O(2)#5	2.347(7)	Er(1)-O(2)#7	2.290(13)	Y(1)-O(2)#7	2.333(10)	Dy(1)-O(2)	2.31(2)
Dy(1)-O(2)#6	2.347(7)	Er(1)-O(2)#8	2.328(8)	Y(1)-O(2)#8	2.379(6)	Dy(1)-O(3)	2.36(6)
Dy(1)-O(3)	2.302(11)	Er(1)-O(2)#2	2.328(8)	Y(1)-O(2)#1	2.379(6)	Dy(1)-O(4)	2.13(4)
Dy(1)-O(3)#1	2.347(7)	Er(1)-O(2)#9	2.328(8)	Y(1)-O(2)#9	2.379(6)	Dy(1)-O(2)#4	2.16(5)
Dy(1)-O(3)#7	2.347(7)	Er(1)-O(2)#10	2.328(8)	Y(1)-O(2)#10	2.379(6)	Dy(1)-O(4)#4	2.33(4)
Dy(1)-O(1)	2.536(13)	Er(1)-O(1)	2.522(16)	Y(1)-O(1)	2.565(12)	Dy(2)-O(1)	2.206(19)
Dy(1)-O(1)#1	2.539(14)	Er(1)-O(1)#11	2.522(16)	Y(1)-O(1)#11	2.565(12)	Dy(2)-O(2)	2.41(6)
Dy(1)-O(1)#7	2.539(14)	Er(1)-O(1)#12	2.522(16)	Y(1)-O(1)#12	2.565(12)	Dy(2)-O(1)#5	2.31(4)
Dy(1)-O(1)#8	2.536(14)	Er(1)-O(1)#2	2.522(16)	Y(1)-O(1)#1	2.565(12)	Dy(2)-O(3) #2	2.27(6)
C(1)-O(1)#1	1.274(13)	C(1)-O(1)#1	1.28(2)	C(1)-O(1)#1	1.311(18)	Dy(2)-O(3) #3	2.25(5)
C(1)-O(1)#2	1.274(13)	C(1)-O(1)#2	1.28(2)	C(1)-O(1)#3	1.311(18)	Dy(2)-O(4)#5	2.40(5)
C(1)-O(1)#3	1.274(13)	C(1)-O(1)#3	1.28(2)	C(1)-O(1)#4	1.311(18)	Dy(3)-O(1)	2.215(19)
C(1)-O(1)#4	1.274(13)	C(1)-O(1)#4	1.28(2)	C(1)-O(1)#5	1.311(18)	Dy(3)-O(3)#3	2.21(5)
C(1)-O(1)	1.274(13)	C(1)-O(1)#5	1.28(2)	C(1)-O(1)#2	1.311(18)	Dy(3)-O(4)#4	2.27(5)
C(1)-O(1)#5	1.274(13)	C(1)-O(1)	1.28(2)	C(1)-O(1)	1.311(18)	Dy(3)-O(2)#3	2.24(5)

Symmetry transformations used to generate equivalent atoms:

For **1**:

#1 -z+3/2,-x+3/2,-y+3/2   #2 y,z,x   #3 -x+3/2,-y+3/2,-z+3/2   #4 z,x,y   #5 -y+3/2,-z+3/2,-x+3/2

#6 y-1/2,-z+3/2,x+1/2   #7 z-1/2,-x+3/2,-y+3/2   #8 -x+1,y,z

For **2**:

#1 -y+1/2,-z+1/2,-x+1/2   #2 -z+1/2,-x+1/2,-y+1/2   #3 z,x,y   #4 y,z,x   #5 -x+1/2,-y+1/2,-z+1/2

#6 -y+1/2,z+1/2,-x+1/2   #7 z,-y+1,x   #8 -y+1/2,-x+1/2,-z+1/2   #9 y-1/2,x+1/2,-z+1/2   #10

-z+1/2,x+1/2,y-1/2   #11 x,-y+1,z   #12 -z+1/2,x+1/2,-y+1/2

For **3**:

#1 -z+1/2,-x+1/2,-y+1/2   #2 -y+1/2,-z+1/2,-x+1/2   #3 y,z,x   #4 -x+1/2,-y+1/2,-z+1/2   #5 z,x,y

#6 -y+1/2,z+1/2,-x+1/2   #7 z,-y+1,x   #8 -y+1/2,-x+1/2,-z+1/2   #9 -z+1/2,x+1/2,y-1/2   #10

y-1/2,x+1/2,-z+1/2   #11 x,-y+1,z   #12 -z+1/2,x+1/2,-y+1/2

For **1-c**:

#1 x-y,x-1,-z+1   #2 -x+y+4/3,-x+2/3,z-1/3   #3 -x+5/3,-y+1/3,-z+4/3   #4 -y+2/3,x-y-2/3,z+1/3

#5 y+1,-x+y+1,-z+1

Table S5. Crystal data and structure refinement for **1-c**[a].

Compound	1-c
Empirical formula	$ClDy_3O_5$
Formula weight	586.95
Temperature	296(2) K
Wavelength (Å)	0.71073
Crystal system, space group	Trigonal, R-3
Unit cell dimensions	
a (Å)	16.64(3)
b (Å)	16.64(3)
c (Å)	10.217(19)
α (°)	90
β (°)	90
γ (°)	120
Volume (Å^3)	2451(8)
Z, calculated density (mg m^{-3})	18, 7.158
Absorption coefficient (mm^{-1})	41.134
F(000)	4446
Crystal size (mm^3)	$0.06 \times 0.06 \times 0.03$
θ range (°) for data collection	2.45 – 24.83
Limiting indices	$-18 \leq h \leq 19$, $-19 \leq k \leq 19$, $-12 \leq l \leq 9$
Reflections collected/unique	3945/894, [R_{int} = 0.1268]
Completeness to θ (%)	24.83, 96.6
Absorption correction	Semi-empirical from equivalents
Max and min transmission	0.3717 and 0.1916
Refinement method	Full-matrix least-squares on F^2
Data/restraints/parameters	894/27/81
Goodness-of-fit on F^2	0.950
Final R indices [$I > 2\sigma(I)$]	$R_1 = 0.0927$, $wR_2 = 0.2245$
R indices (all data)	$R_1 = 0.2356$, $wR_2 = 0.3476$
Largest diff. peak and hole (e Å^{-3})	4.214 and -2.427

[a] $R_1 = \sum(\Delta F/\sum(F_o))$, $wR_2 = (\sum[w(F_o^2 - F_c^2)])/\sum[w(F_o^2)^2]^{1/2}$ and $w = 1/\sigma^2(F_o^2)$.
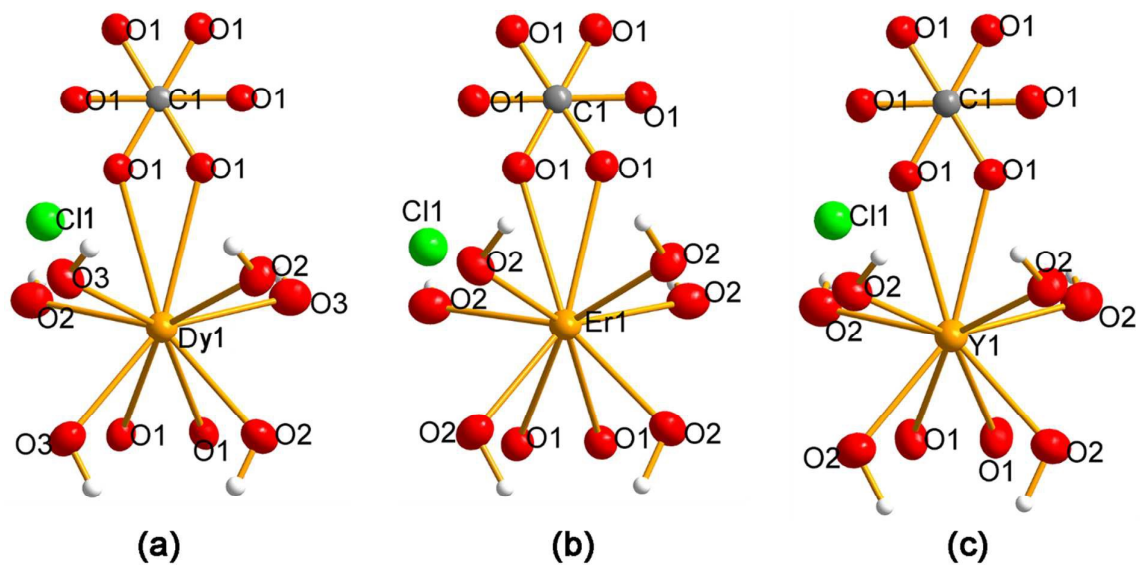
Fig. S1 Thermal ellipsoids given at 50% probability, showing the atomic labeling scheme of **1**, **2** and **3**, with white H atoms signed as white balls.
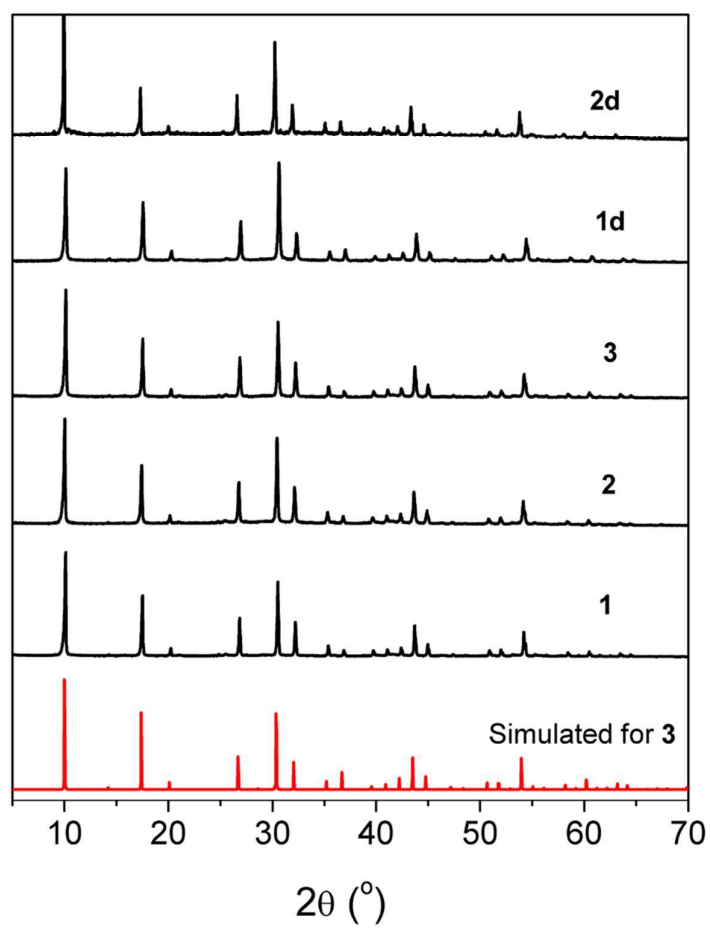
Fig. S2 Experimental PXRD patterns of **1**, **2**, **3**, **1d** and **2d**, comparing with the simulated one for **3**.
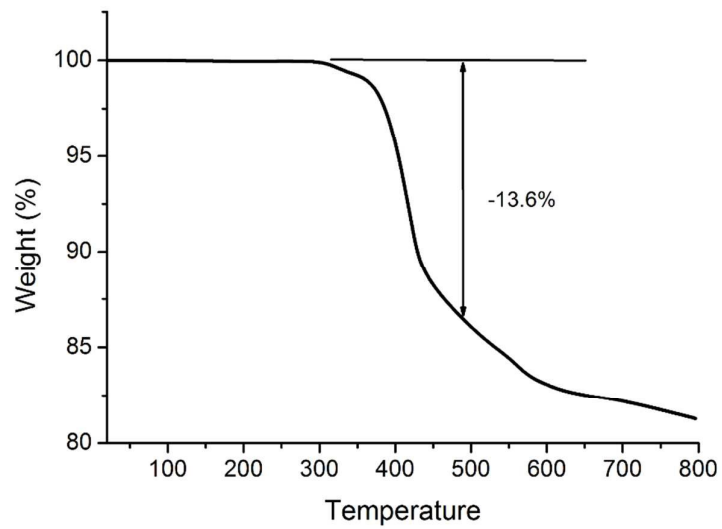
Fig. S3 TGA curves of as-synthesized **1**.
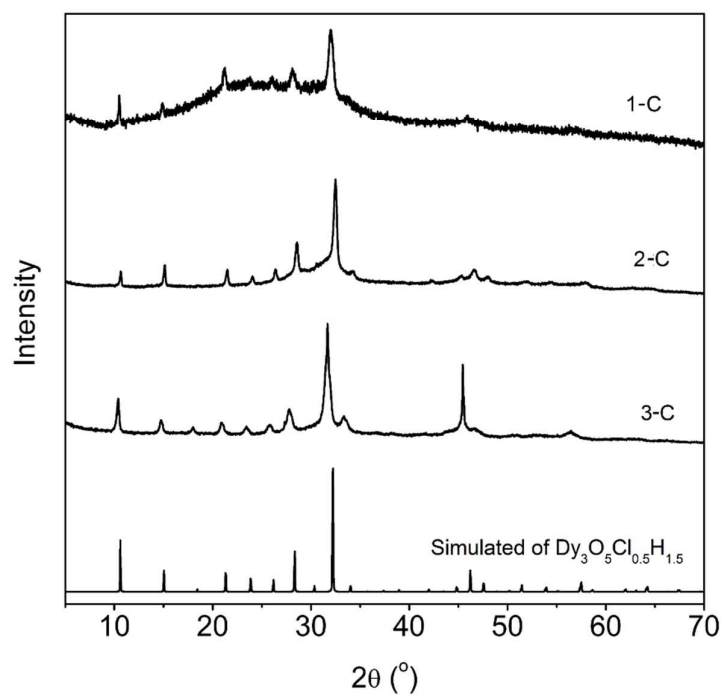
Fig. S4 Experimental PXRD for **1-c**, **2-c** and **3-c** and simulated PXRD pattern of **1-c**.
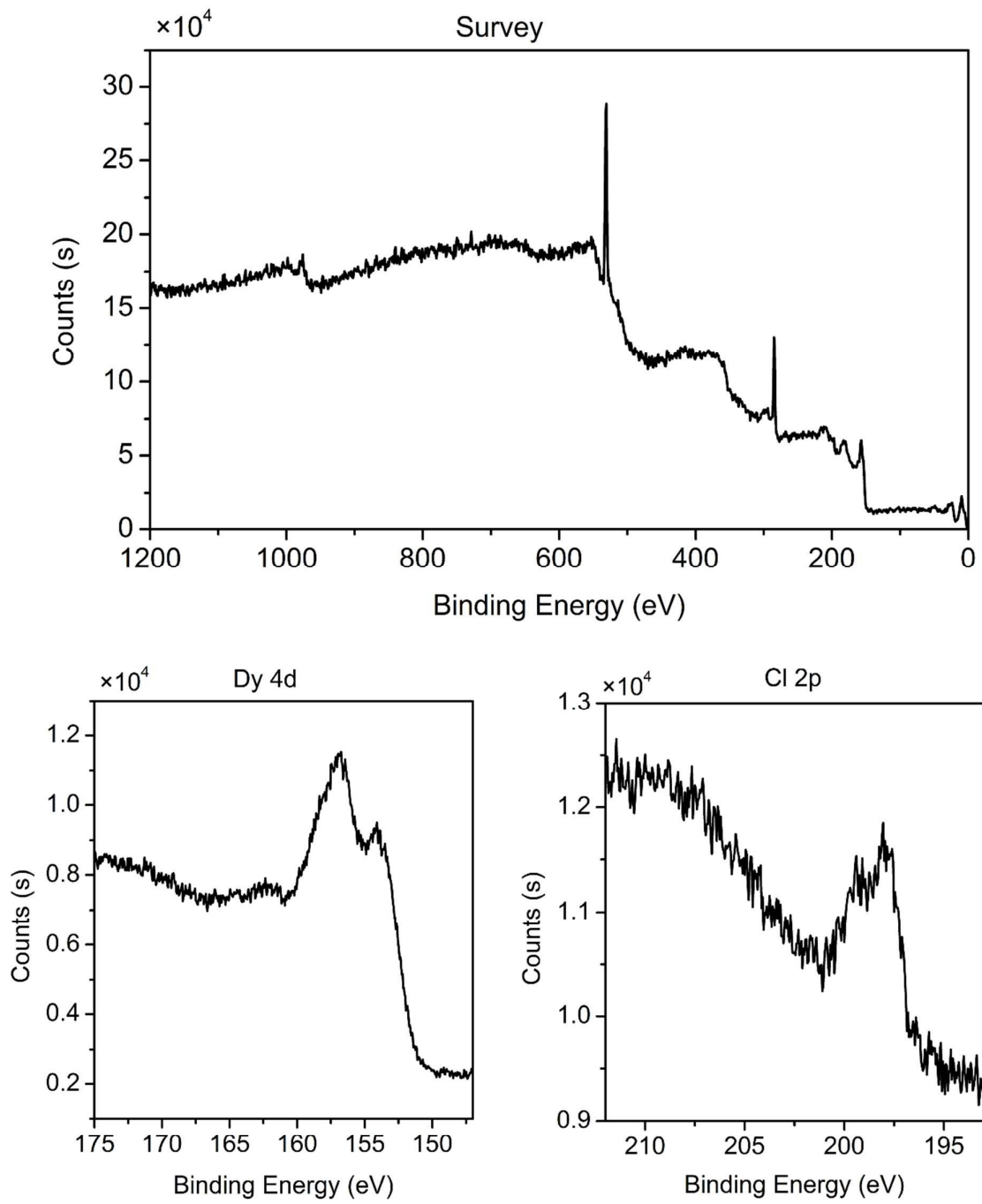
(a)
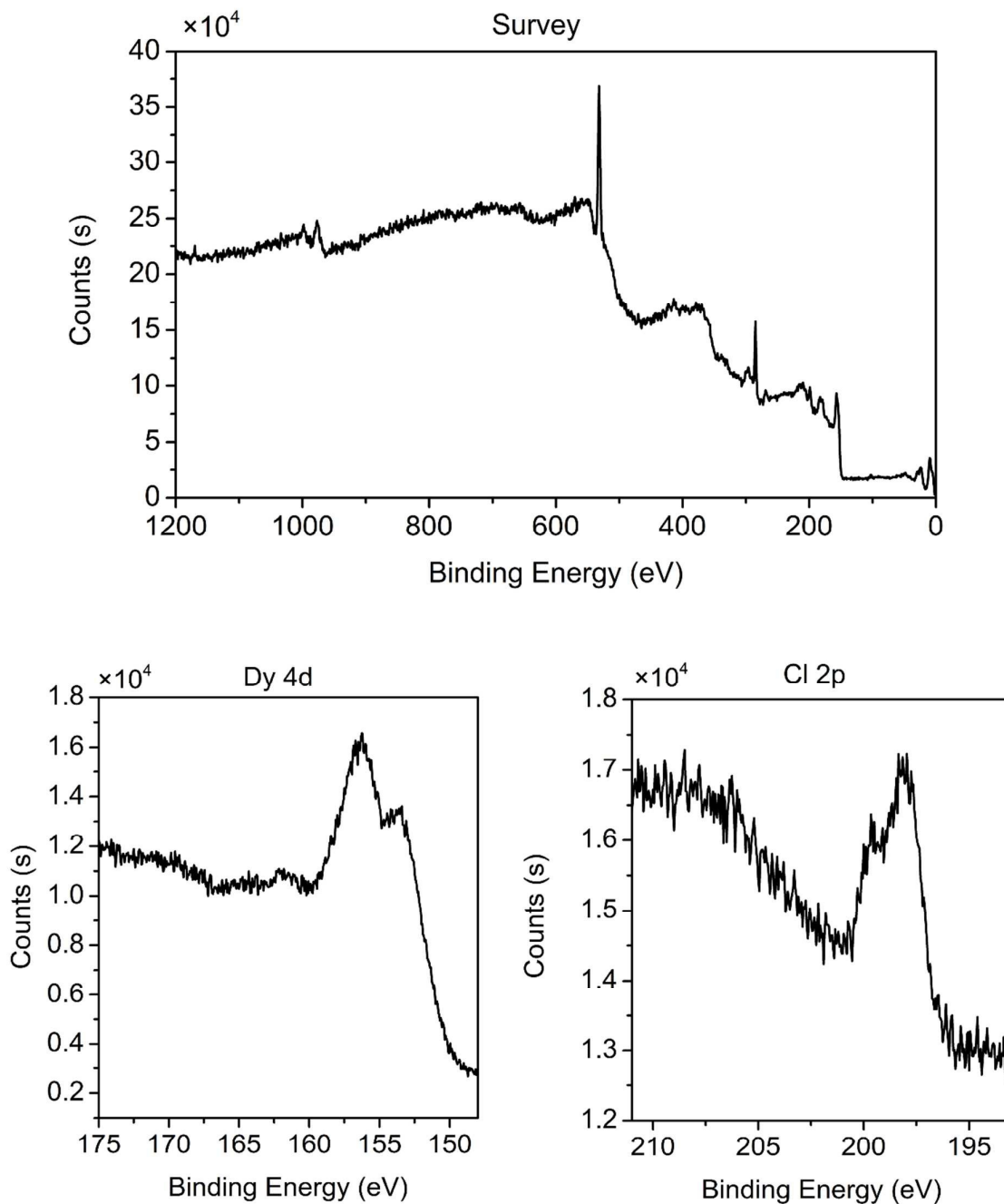
(b)

Fig. S5 X-ray photoelectron spectra of (a) **1** and (b) **1-c**, the signal around 198 eV, which corresponding to Cl 2p, indicating the existence of Cl for the crystals.
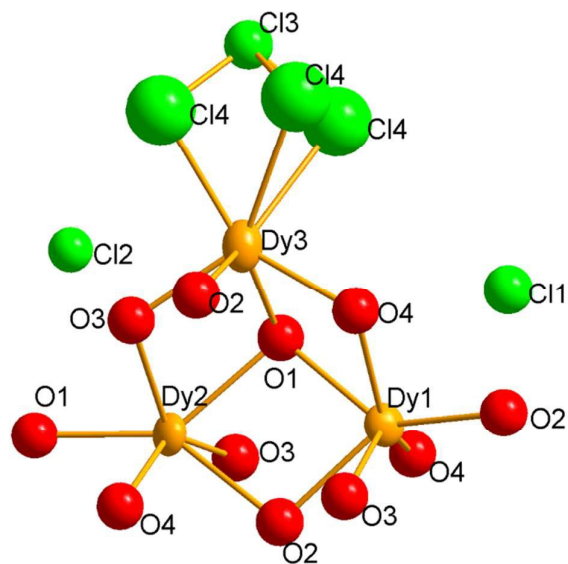
Fig. S6 Asymmetric unit of **1-c**, shows three crystallographically distinct of Dy atoms.
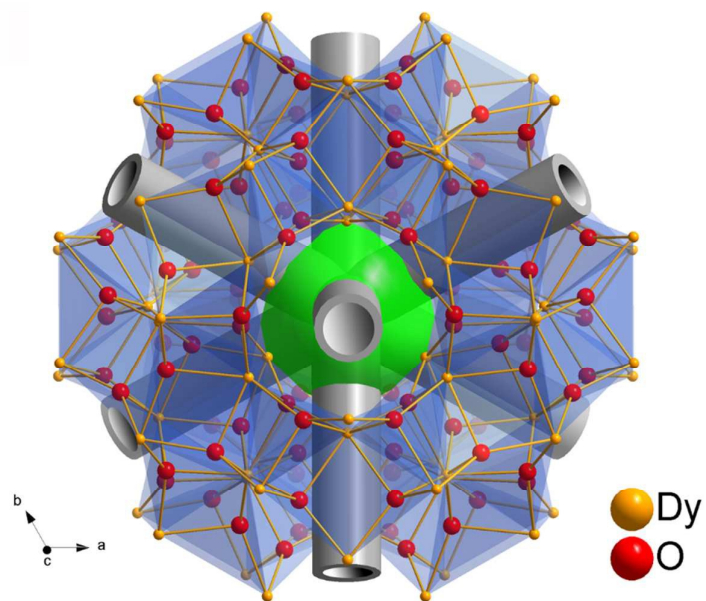
Fig. S7 Structure of **1-c** along [001] direction, with 3-D intersection 6-ring channels along [001], [1 11], [211] and [121].
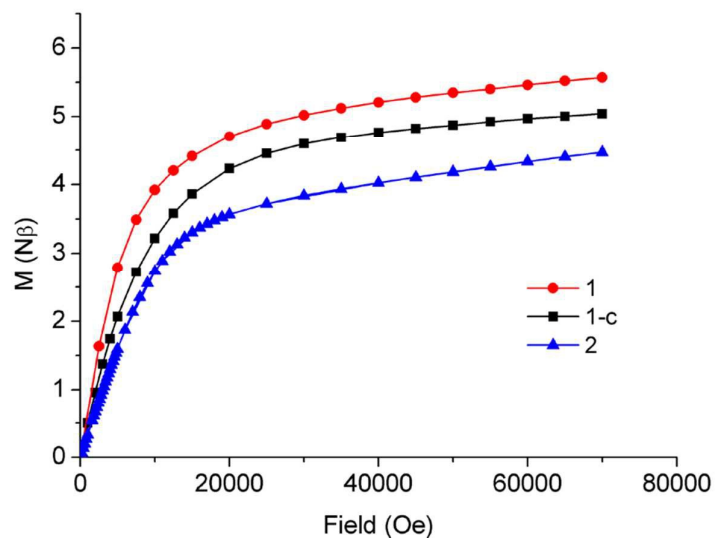
Fig. S8 M-H curve for (a) **1**; (b) **1-c** and (c) **2** at 2.00 K.
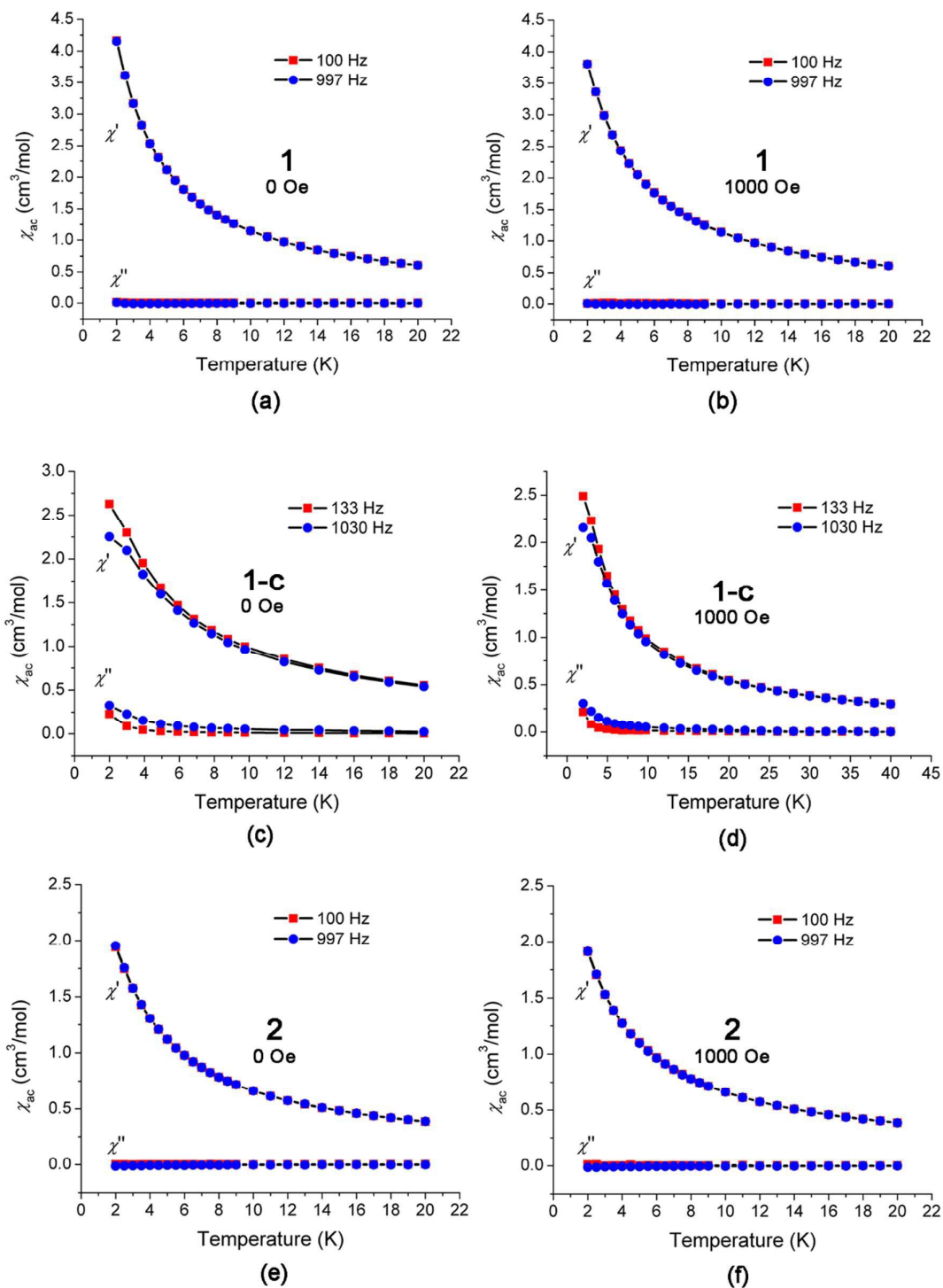
Fig. S9 Temperature-dependent in-phase (χ'_M) (up) and out-of-phase (χ''_M) (down) ac susceptibility components at different frequencies for complex **1** ((a) and (b)), **1-c** ((c) and (d)) and **2** ((e) and (f)) with applied dc field of 0 Oe (left) and 1000 Oe (right). The solid lines join the data points.
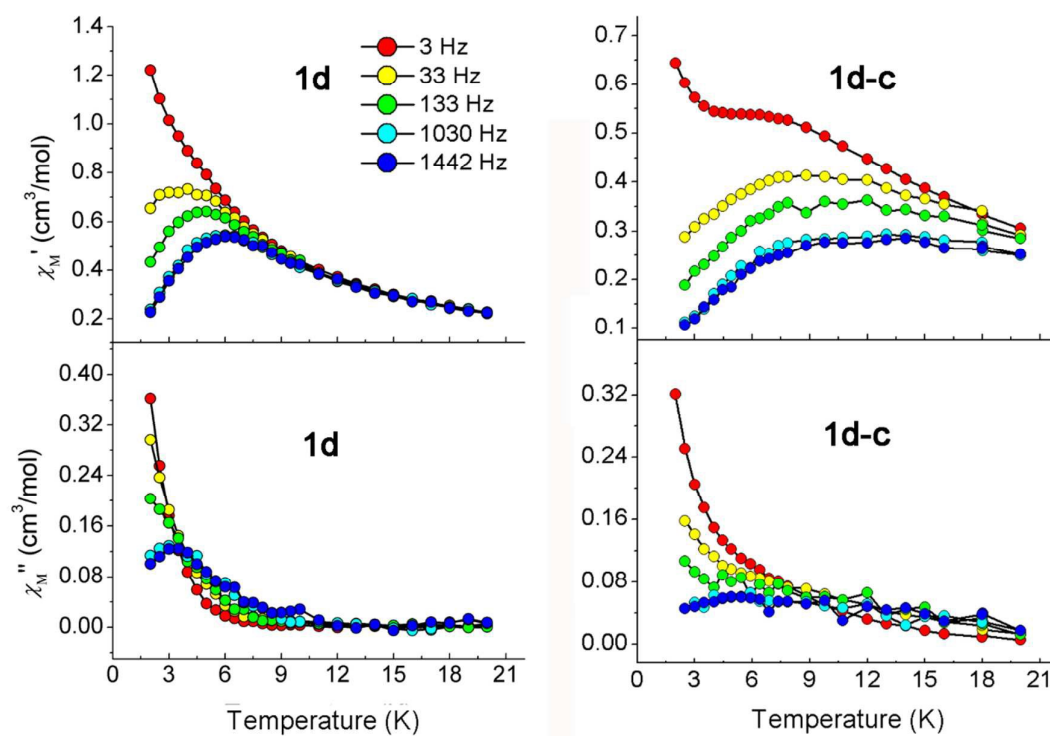
Fig. S10 Temperature dependent in-phase (χ'_M) (up) and out-of-phase (χ''_M) (down) ac susceptibility components at different frequencies for the diluted sample **1d** (with Dy/Y = 1/440) and the corresponding calcined sample **1d-c** with 500 Oe applied dc field. The solid lines join the data points.
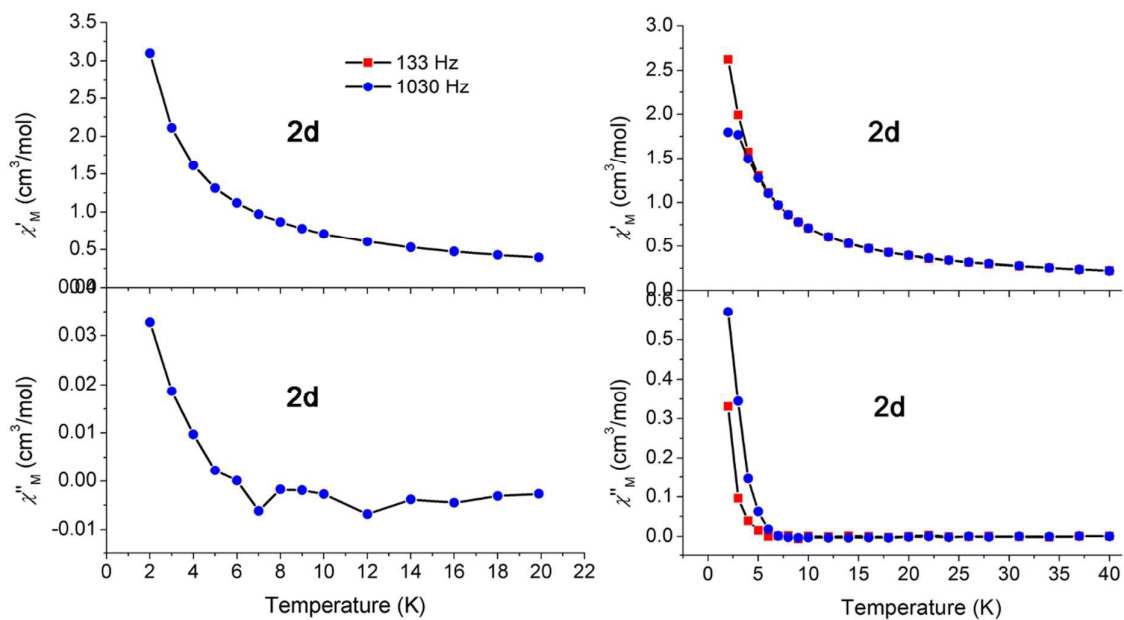
Fig. S11 Temperature dependent in-phase (χ'_M) (up) and out-of-phase (χ''_M) (down) AC susceptibility components at different frequencies for the diluted sample **2d** (with Er/Y = 1/15) with applied DC field of 0 Oe (left) and 1000 Oe (right). The solid lines join the data points. Ac in the presence of a small external dc field of 1000 Oe show the presence of an out-of-phase signal, χ'', for **2d** in contrast with **2**.